Electronic Supplementary Information

Interplay of a Nitro-group and Metal Ions: from Coordinative Binding to Noncovalent Semicoordination

Vitalii V. Suslonov,[1,2,3] Natalia S. Soldatova,[2] Daniil M. Ivanov,[1,2] Pavel S. Postnikov,[2] Rosa M. Gomila,[4] Antonio Frontera,[4] Vadim Yu. Kukushkin,*[1,5] Nadezhda A. Bokach*[1,2]

[1] Saint Petersburg State University, 7/9 Universitetskaya Nab., Saint Petersburg 199034, Russian Federation

[2] Research School of Chemistry and Applied Biomedical Sciences, Tomsk Polytechnic University, Tomsk 634034, Russian Federation

[3] S.M. Kirov Academy, Akad. Lebedeva St., 6, Saint Petersburg 194044, Russian Federation

[4] Departament de Química, Universitat de les Illes Balears, Crta. de Valldemossa km 7.5, 07122 Palma de Mallorca (Baleares), Spain

[5] Institute of Chemistry and Pharmaceutical Technologies, Altai State University, 656049 Barnaul, Russian Federation

Emails: v.kukushkin@spbu.ru; n.bokach@spbu.ru

*Corresponding authors

Table of contents

S1. XRD data 2
S2. Consideration of the structures 3
S3. Hirshfeld surface analysis 7
S4. CSD search results 9
S5. Theoretical studies 14
S6. Crystallization and characterization of **1**–**3** 15
S7. Experimental data 17
References 28

S1. XRD data

Table S1. Crystal data and structure refinement for **1**·CH_2Cl_2, **2**·$MeNO_2$, and **3**·$MeNO_2$.

Identification code	**1**·CH_2Cl_2	**2**·$MeNO_2$	**3**·$MeNO_2$
Empirical formula	$C_{35}H_{32}Cl_2I_2N_6NiO_{10}$	$C_{35}H_{33}I_2N_7O_{12}Pd$	$C_{35}H_{33}I_2N_7O_{12}Pt$
Formula weight	1080.07	1103.88	1192.57
Temperature/K	100(2)	100(2)	100(2)
Crystal system	monoclinic	monoclinic	monoclinic
Space group	C2/c	C2/c	C2/c
a/Å	22.4636(5)	22.5407(2)	22.5831(3)
b/Å	12.6983(3)	12.83600(10)	12.8189(2)
c/Å	13.5865(2)	13.66040(10)	13.6642(2)
α/°	90	90	90
β/°	98.051(2)	97.8870(10)	98.0300(10)
γ/°	90	90	90
Volume/Å^3	3837.33(14)	3915.01(6)	3916.87(10)
Z	4	4	4
ρ_{calc}g/cm^3	1.870	1.873	2.022
μ/mm^{-1}	15.207	16.820	5.230
F(000)	2128.0	2160.0	2288.0
Crystal size/mm^3	0.25 × 0.2 × 0.2	0.2 × 0.15 × 0.1	0.2 × 0.15 × 0.12
Radiation	CuKα (λ = 1.54184)	CuKα (λ = 1.54184)	MoKα (λ = 0.71073)
2Θ range for data collection/°	7.95 to 139.98	7.92 to 139.978	6.022 to 54.98
Index ranges	–27 ≤ h ≤ 27 –13 ≤ k ≤ 15 –16 ≤ l ≤ 15	–27 ≤ h ≤ 27 –15 ≤ k ≤ 15 –15 ≤ l ≤ 16	–28 ≤ h ≤ 19 –15 ≤ k ≤ 16 –15 ≤ l ≤ 17
Reflections collected	16864	49287	8309
Independent reflections	3639 [R_{int} = 0.0562, R_{sigma} = 0.0323]	3723 [R_{int} = 0.0494, R_{sigma} = 0.0152]	4307 [R_{int} = 0.0179, R_{sigma} = 0.0257]
Data/restraints/parameters	3639/0/258	3723/0/259	4307/0/286
Goodness-of-fit on F^2	1.040	1.089	1.043
Final R indexes [I>=2σ (I)]	R_1 = 0.0381, wR_2 = 0.1029	R_1 = 0.0264, wR_2 = 0.0735	R_1 = 0.0184, wR_2 = 0.0415
Final R indexes [all data]	R_1 = 0.0401, wR_2 = 0.1056	R_1 = 0.0267, wR_2 = 0.0738	R_1 = 0.0216, wR_2 = 0.0429
Largest diff. peak/hole / e Å^{-3}	2.56/–1.19	0.73/–1.00	0.67/–0.74
CCDC Nos	2304939	2304940	2304938

S2. Consideration of the structures

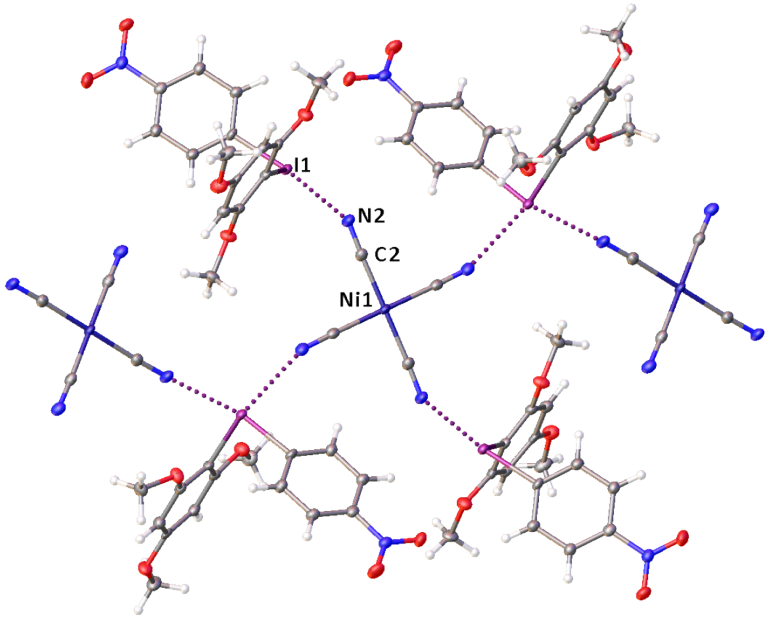

Figure S1. A fragment of the HaB-based crystal packing of **1**·CH_2Cl_2; CH_2Cl_2 was omitted for simplicity.

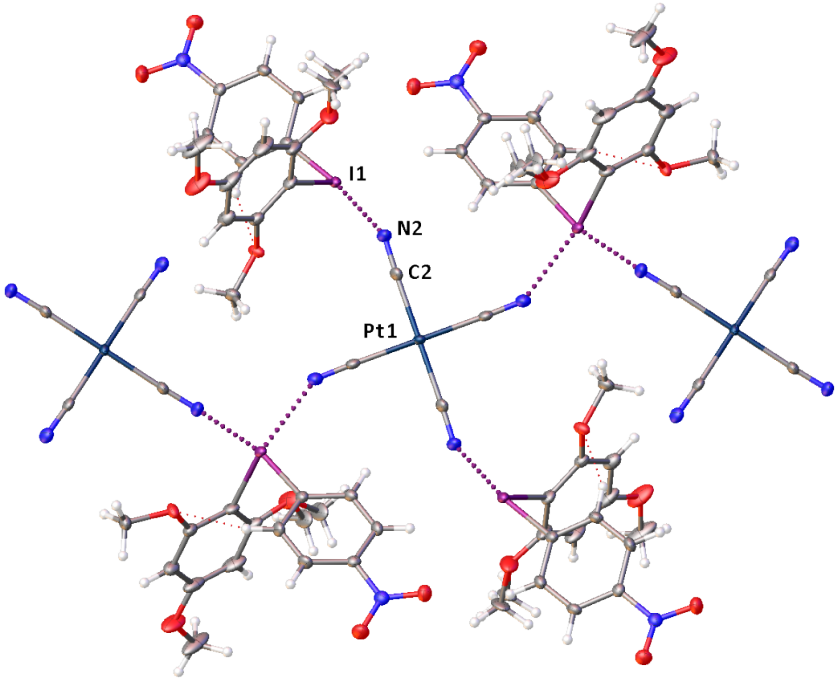

Figure S2. A fragment of the HaB-based crystal packing of **3**·$MeNO_2$; $MeNO_2$ was omitted for simplicity.

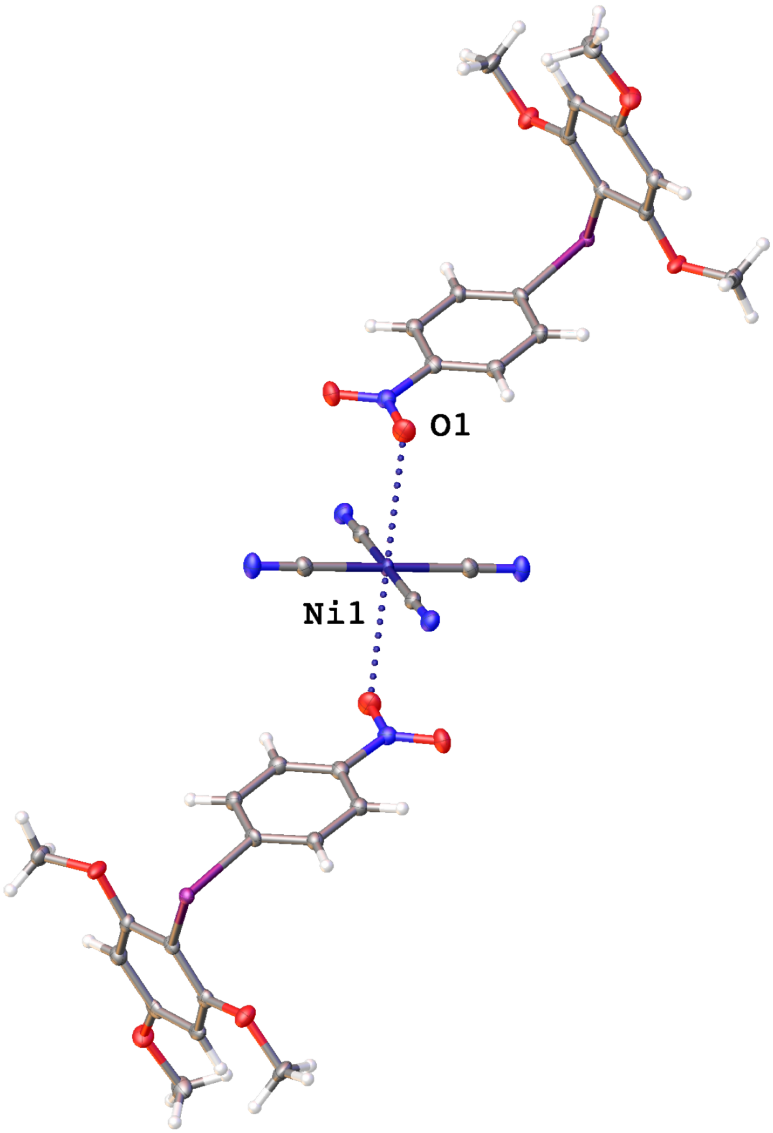

Figure S3. A fragment of the crystal packing of **1**·CH_2Cl_2 showing semicoordination (dotted lines); CH_2Cl_2 was omitted for simplicity.

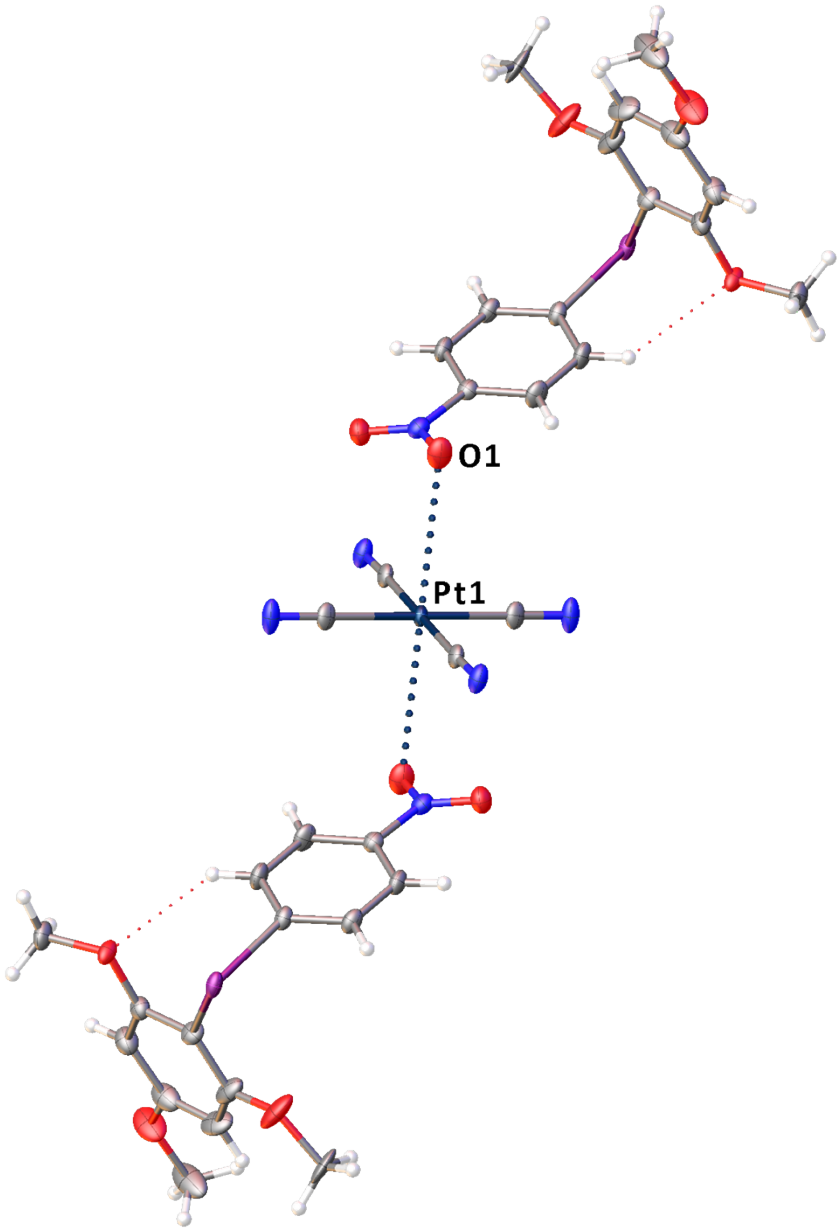

Figure S4. A fragment of the crystal packing of **3**·$MeNO_2$ showing semicoordination (dotted lines); $MeNO_2$ was omitted for simplicity.

All XRD structures are composed of the anion $[M(CN)_4]^{2-}$ and two $[Ar^1Ar^2I]^+$ cations and display almost the same HaB-based motif, which includes pseudo-layered architecture (**Figures 1**, **S1** and **2S**; **Figure S5**, **a**). This pattern differs from those previously observed for $[Ph_2I]_2[M(CN)_4]$ (M = Ni, Pd)[1] and $[Ar^1Ar^2I]_2[PtCl_4]$.[2, 3] Thus, the complex $[Ph_2I]_2[M(CN)_4]$, bearing unsubstituted diaryliodonium cation, forms I···N HaB-based infinite chains with shared vertexes occupied by the $[M(CN)_4]^{2-}$ anions (**Figure S5**, **b**). Structures of $[Ar^1Ar^2I]_2[PtCl_4]$ are represented by heterotrimers (**Figure S5**, **c**). The latter difference between supramolecular motifs is probably related to the difference in interatomic distances between the *cis*-$(N)_2$ and *cis*-$(Cl)_2$ nucleophilic centers in the anionic metalates. The differences in the anisotropic distribution of the electron density around these two elements in the respective anions also play a significant role. At

the same time, common feature for all four ligands of each complex is that they are involved in HaB.

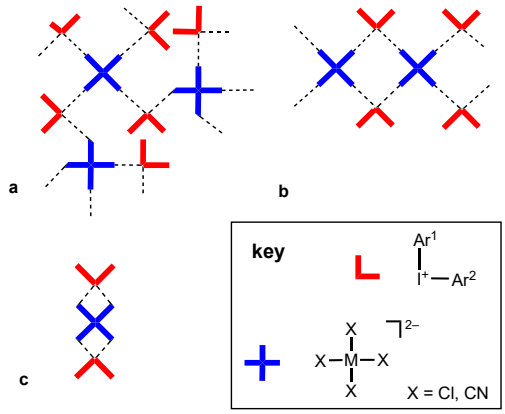

Figure S5. Schematic representation of main HaB-based structural motifs for $[Ar^1Ar^2I]_2[M(CN)_4]$ (M = Ni, Pd, Pt) (*a*), $[Ph_2I]_2[M(CN)_4]$ (M = Ni, Pd) (*b*), and $[Ar^1Ar^2I]_2[PtCl_4]$ (*c*).

The common contact type for the three structures under study is the I···N HaB occurred between the I atom of the iodonium cation and N atom of a CN^- ligand; all observed contacts fulfill the IUPAC criteria[4] for the identification of HaB, which belong to Type-II[4] halogen-halogen interactions (**Table S2**). The I···N distances are in the range 2.78–2.94 Å and the shortest separations (2.768(3) Å; 78% of Bondi Σ_{vdW} I + N were observed for **2**. The ∠C–I–N angles (168–171°) tend to linear. Each iodonium cation form two 2-center HaBs because the iodine atom exhibits two σ-holes on the extension of each C–I covalent bonds.

Table S2. I···N HaB in the structures of $[Ar^1Ar^2I]_2[M(CN)_4]$.

Nos	**Contact**	**d(I···N), Å**	**∠C–I···N,°**	**∠I···N–C,°**
1	C3–I1···N2–C2	2.780(3)	168.46(13)	140.1(3)
	C9–I1···N1–C1	2.921(4)	168.88(10)	140.1(3)
2·$MeNO_2$	C3–I1···N2–C2	2.768(3)	168.97(9)	138.7(3)
	C12–I1···N1–C1	2.931(3)	171.28(9)	136.6(2)
3·$MeNO_2$	C3–I1···N2–C2	2.775(2)	168.75(8)	138.3(2)
	C9–I1···N1–C1	2.936(2)	171.43(8)	135.9(2)

[a] R_{Bondi}[5] = d/Σ_{vdW}; Bondi Σ_{vdW} I + N = 3.53 Å.

The nitro group forms short contacts with solvent molecules (CH_2Cl_2 or $MeNO_2$). These contacts occurred between the N-atom and Cl/O-atoms from the solvent. These contacts can be recognized as π-hole$_{NO2}$···lone pair(Cl/O) interactions.

Table S3. The π-hole$_{NO2}$···Cl/O contacts in the studied structures.

Structure	Contact	Distance, Å (Nc)	Angle C–N–X, °	Angle N–X–Y, °
1·CH_2Cl_2	N3–Cl1S	3.301(3) (1.00)	83.9(2)	98.08(8)
2·$MeNO_2$	N3–O2S	2.955(7) (0.96)	90.52(19)	104.1(4)
3·$MeNO_2$	N3–O2S	2.948(10) (0.96)	89.3(3)	100.4(9)

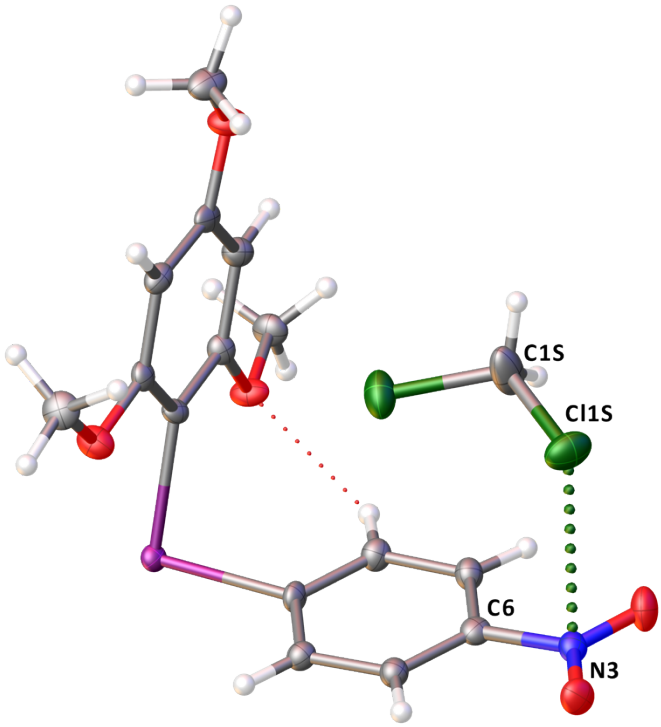

Figure S6. π-hole$_{NO2}$···Cl contact in the structure of **1**·CH_2Cl_2.

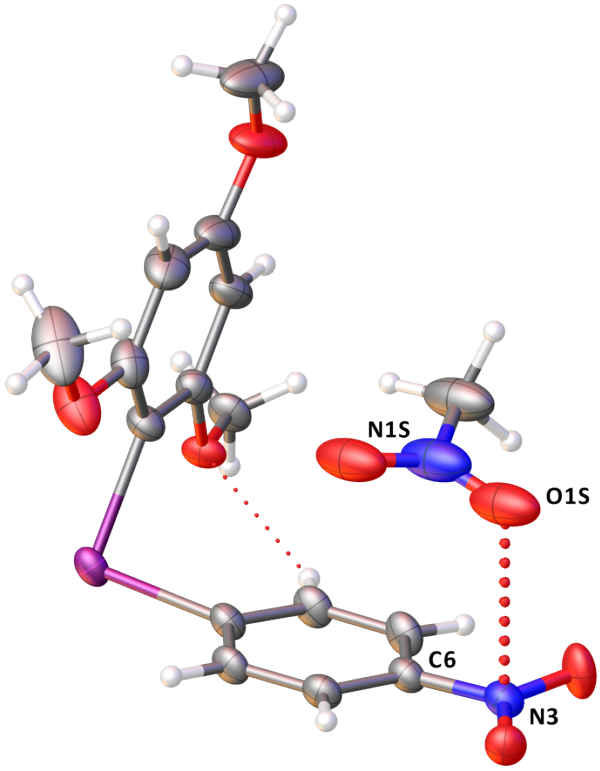

Figure S7. π-hole$_{NO2}$···O contact in the structure of **2**·$MeNO_2$.

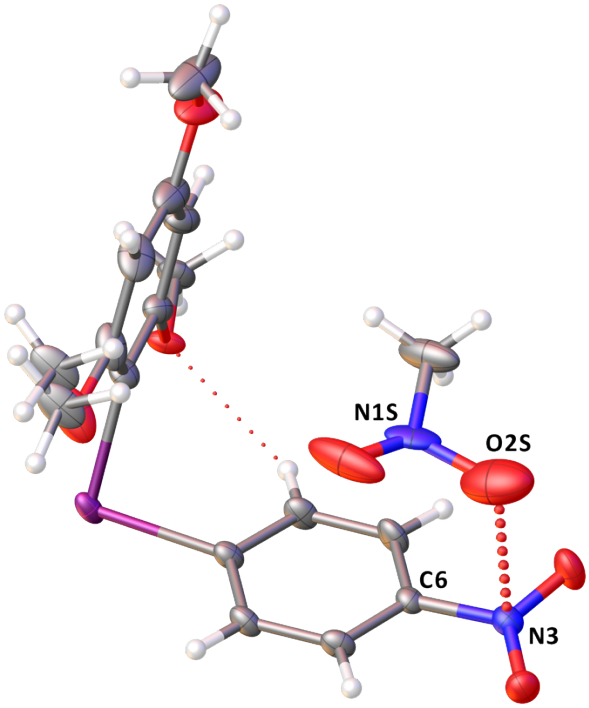

Figure S8. π-hole$_{NO2}$···Cl contact in the structure of **3**·$MeNO_2$.

S3. Hirshfeld surface analysis

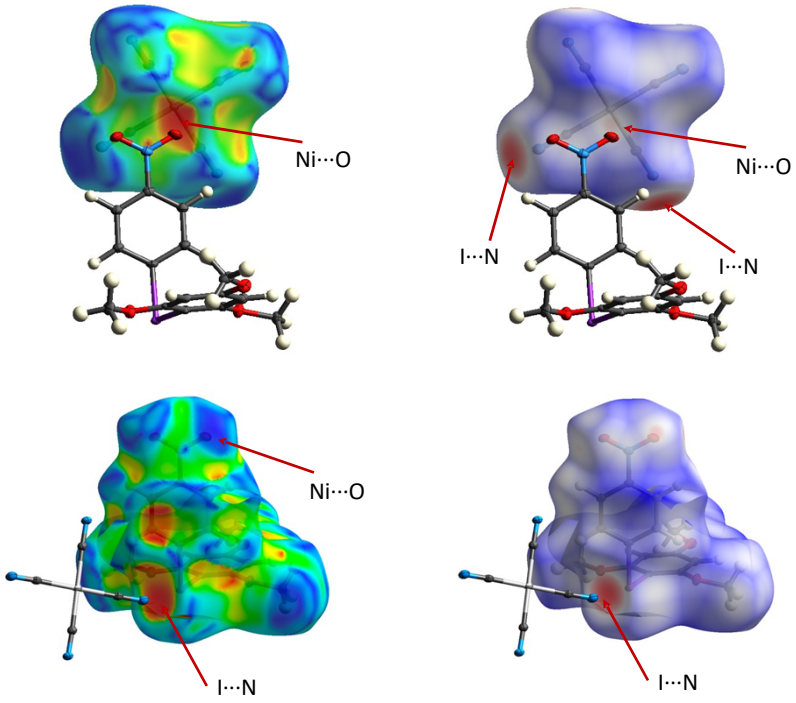

Figure S9. Hirshfeld surface of $[Ni(CN)_4]^{2-}$ (top) and $[\{2,4,6\text{-}(MeO)_3C_6H_2\}(4\text{-}NO_2\text{-}C_6H_4)I]^+$ (bottom) in the structure of **1**·CH_2Cl_2 mapped with shape index (left panel; the presence of red and blue triangles in the center of the anion, in which the red and blue color represent the bumps and hollow regions on the shape index surfaces, respectively) and d_{norm} (right panel) showing the Ni···O short contact and I···N HaBs.

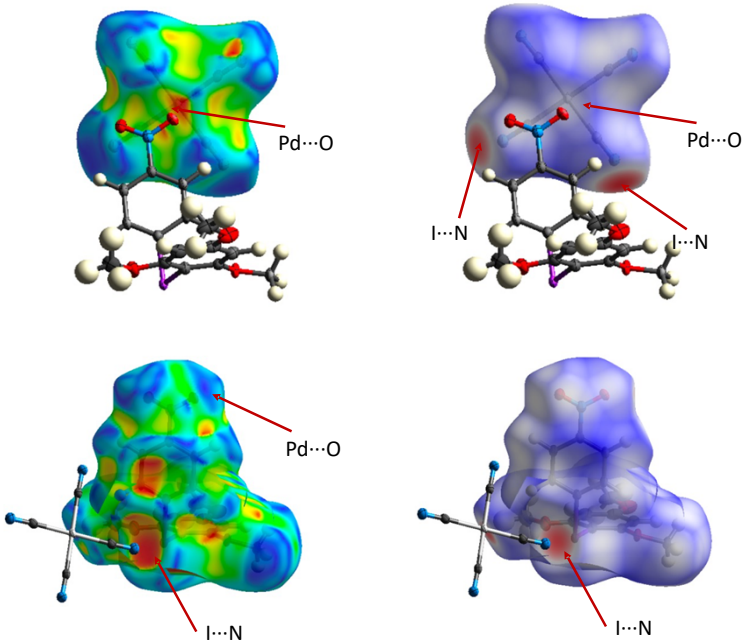

Figure S10. Hirshfeld surface of $[Pd(CN)_4]^{2-}$ (top) and $[\{2,4,6\text{-}(MeO)_3C_6H_2\}(4\text{-}NO_2\text{-}C_6H_4)I]^+$ (bottom) in the structure of **2**·$MeNO_2$ mapped with shape index (left panel) and d_{norm} (right panel) showing the Pd···O short contact and I···N HaBs.

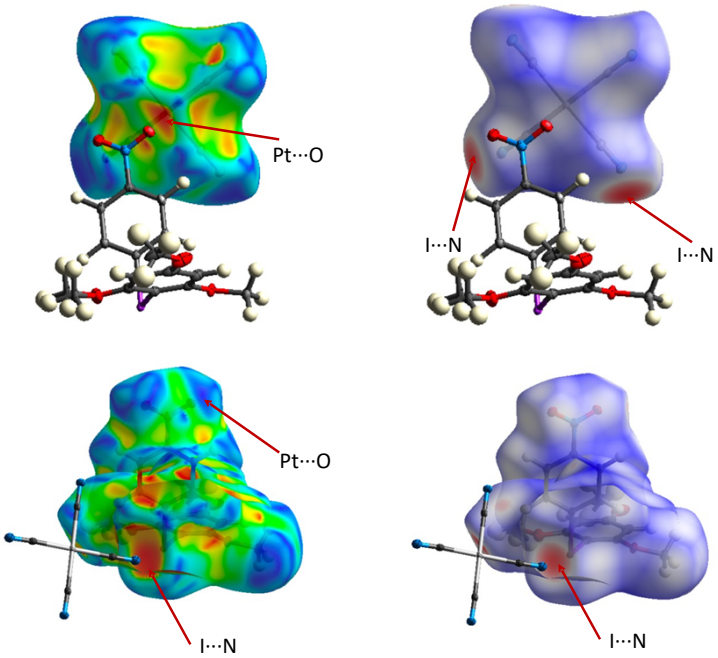

Figure S11. Hirshfeld surface of $[Pt(CN)_4]^{2-}$ (top) and $[\{2,4,6\text{-}(MeO)_3C_6H_2\}(4\text{-}NO_2\text{-}C_6H_4)I]^+$ (bottom) in the structure of **3**·$MeNO_2$ mapped with shape index (left panel) and d_{norm} (right panel) showing the Pt···O short contact and I···N HaBs.

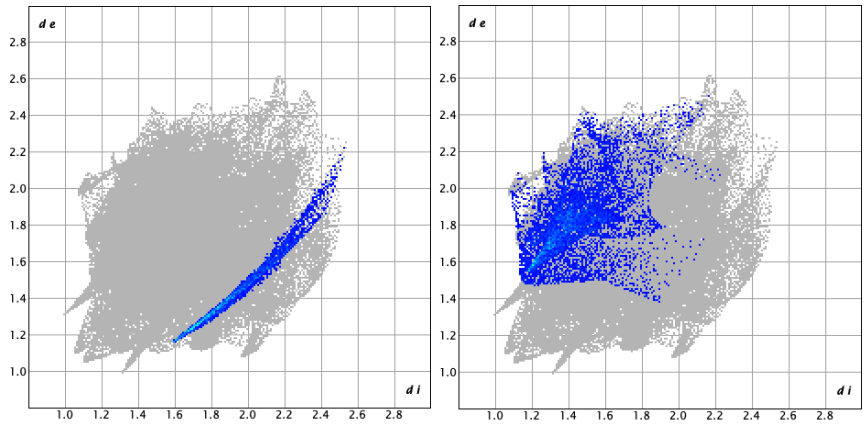

Figure S12. The 2D-fingerprint of the Hirshfeld surface of the cation in the structure of **1**·CH_2Cl_2 demonstrating I···N (left) and H···N (right) contacts. No reciprocal contacts are provided.

Comments: Narrow wing in the bottom-right corner (3% of the surface area; left panel) corresponds to I···N HaB. Wide cloud (8.4% of the surface area; right figure) is due to different types of H···N contacts including presumably weak attractive C–H···N HBs.

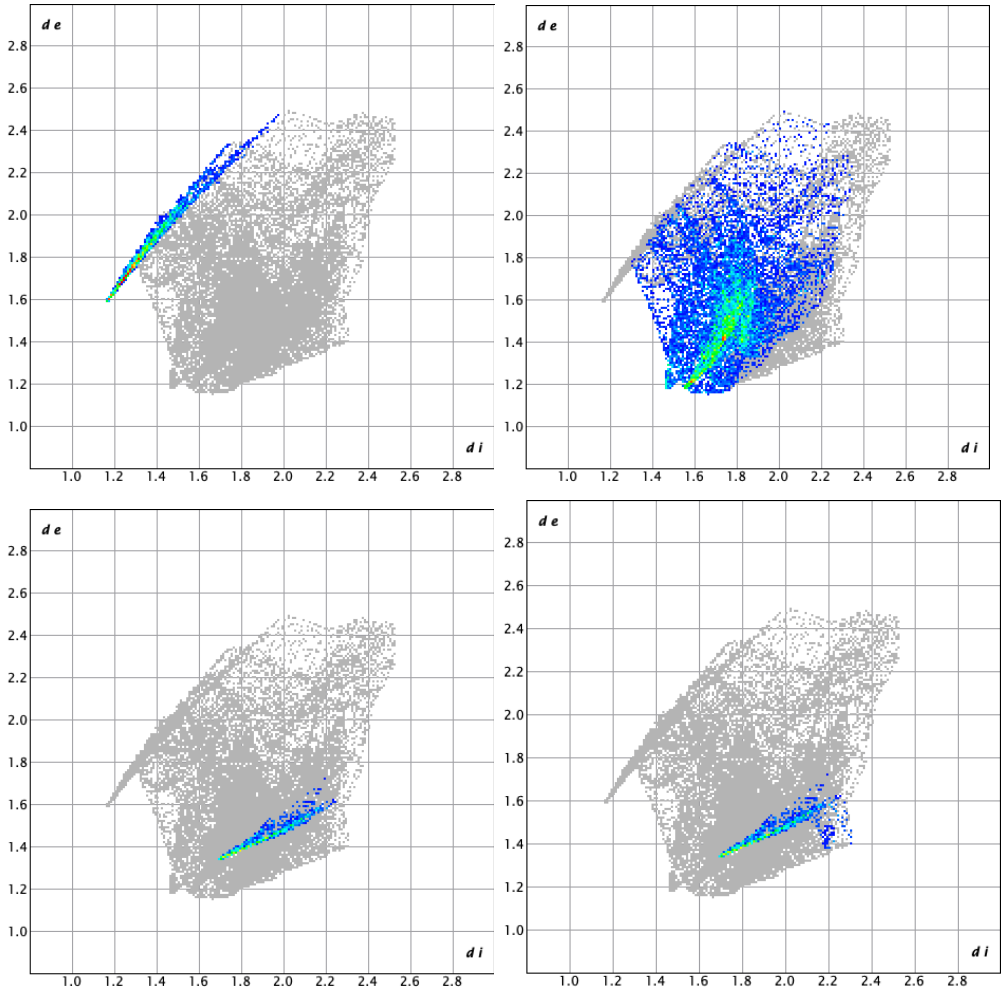

Figure S13. The 2D-fingerprint of the Hirshfeld surface of the anion in the structure of **1**·CH_2Cl_2 demonstrating N···I (top-left), N···H (top-right), Ni···O (bottom-left), and Ni···all atoms (bottom-right) contacts. No reciprocal contacts are provided.

Comments:

Top-left: Narrow spike in the top-left corner (8.7% of the surface area) corresponds to I···N HaB.

Top-right: Wide cloud (right figure; 45.7% of the surface area) is due to different types of H···N contacts, including presumably weak attractive C–H···N HBs (greenish area).

Bottom-left: Narrow spike in the bottom-right corner corresponds to Ni···O contact (4.3% of the surface area).

Bottom-right: In comparison with the previous figure, this figure indicates that Ni···O contact is one of the most significant which involve the Ni atom. Contacts of Ni with all other external atoms

include only 4.7% of the surface area. Apart from Ni···O, other less important interactions include Ni···H contacts.

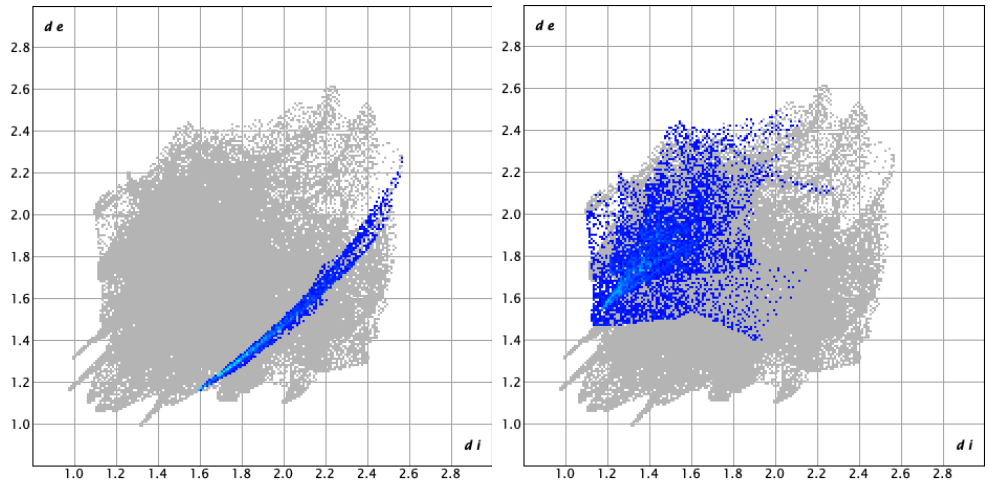

Figure S14. The 2D-fingerprint of the Hirshfeld surface of the cation in the structure of **2**·$MeNO_2$ demonstrating I···N (left) and H···N (right) contacts. No reciprocal contacts are provided.

Comments: Narrow wing in the bottom-right corner (3% of the surface area; left panel) corresponds to I···N HaB. Wide cloud (8.4% of the surface area; right panel) is due to different types of H···N contacts including presumably weak attractive C–H···N HBs.

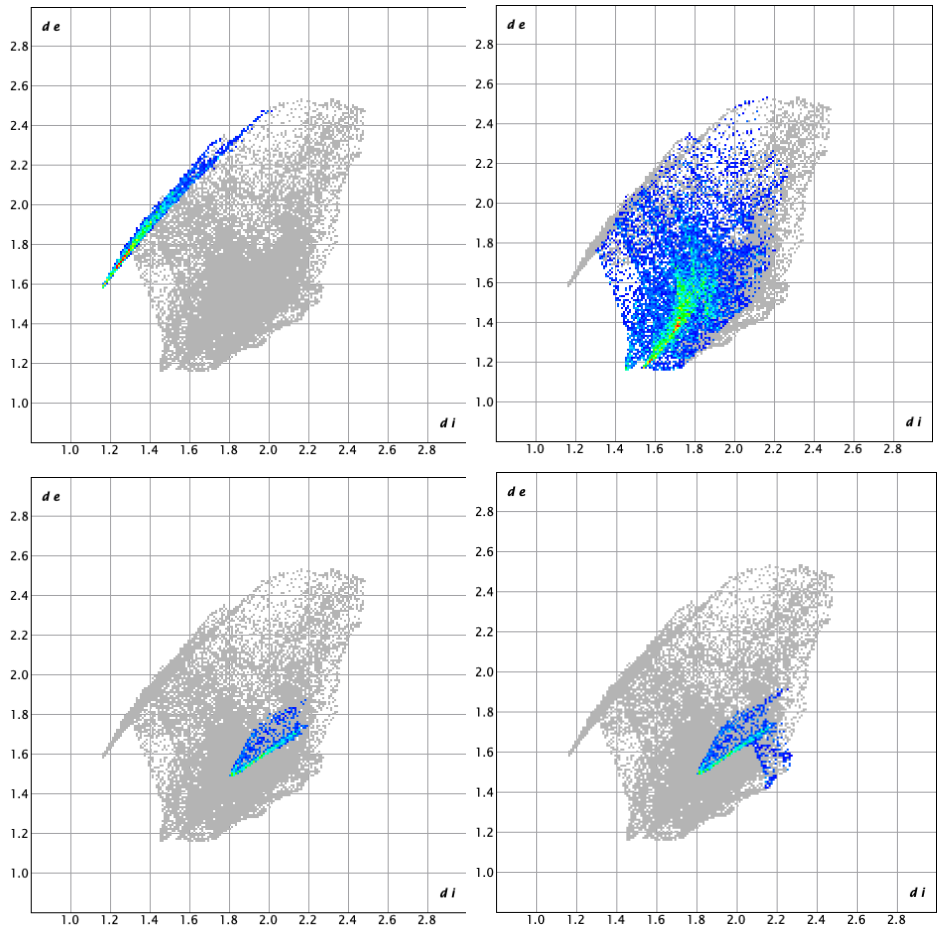

Figure S15. The 2D-fingerprint of the Hirshfeld surface of the anion in the structure of **2**·$MeNO_2$ demonstrating N···I (top-left), N···H (top-right), Pd···O (bottom-left), and Pd···all atoms (bottom-right), contacts. No reciprocal contacts are provided.

Comments:

Top-left: Narrow spike in the top-left corner (8.7% of the surface area) corresponds to I···N HaB.

Top-right: Wide cloud (right figure; 44.0% of the surface area) is due to different types of H···N contacts including presumably weak attractive C–H···N HBs (greenish area).

Bottom-left: The spike in the bottom-right corner corresponds to Pd···O contact (4.1% of the surface area).

Bottom-right: In comparison with the previous figure, this figure indicates that Pd···O contact is one of the most significant which include Pd atom. Contacts of Pdi center with all other external atoms involves 5.1% of the surface area. Apart Pd···O, other less important contacts include Pd···H.

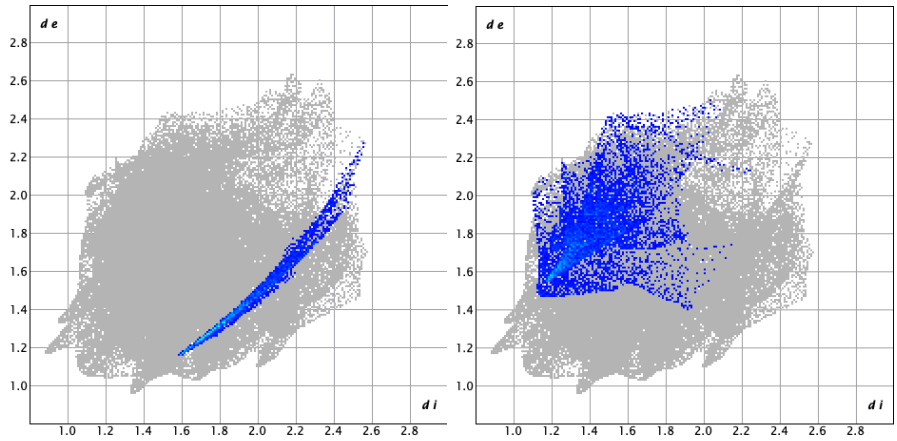

Figure S16. The 2D-fingerprint of the Hirshfeld surface of the cation in the structure of **3**·$MeNO_2$ demonstrating I···N (left) and H···N (right) contacts. No reciprocal contacts are provided.

Comments: Narrow wing in the bottom-right corner (3.1% of the surface area; left panel) corresponds to I···N HaB. Wide cloud (8.4% of the surface area; right panel) is due to different types of H···N contacts including presumably weak attractive C–H···N HBs.

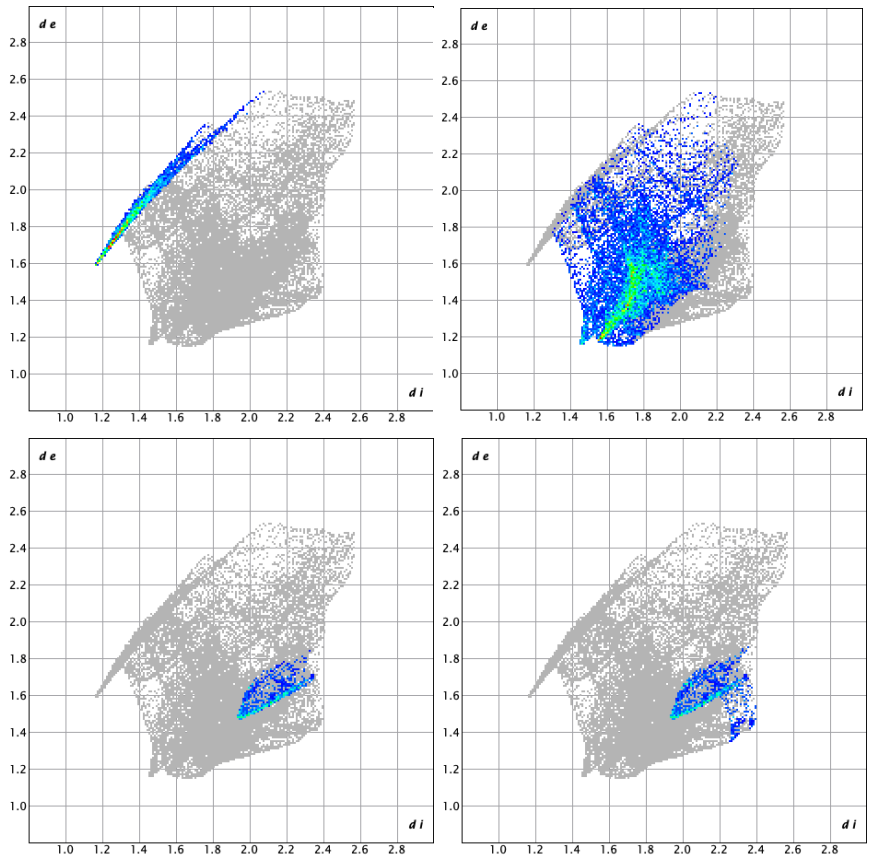

Figure S17. The 2D-fingerprint of the Hirshfeld surface of the anion in the structure of **3**·$MeNO_2$ demonstrating N···I (top-left), N···H (top-right), Pt···O (bottom-left), and Pt···all atoms (right bottom) contacts. No reciprocal contacts are provided.

Comments:

Top-left: Narrow spike in the top-left corner (8.6% of the surface area) corresponds to I···N HaB.

Top-right: Wide cloud (right figure; 44.1% of the surface area) is due to different types of H···N contacts including presumably weak attractive C–H···N HBs (greenish area).

Bottom-left: Wide spike in the bottom-right corner corresponds to Pt···O contact (3.8% of the surface area).

Bottom-right: In comparison with the previous figure, this figure indicates that Pt···O contact is one of the most significant which include the Pt atom. Contacts of Pt center with all other external atoms involves 5.1% of the surface area. Apart from Pd···O, other less important contacts include Pd···H.

S4. CSD search results

Table S4. CSD data for M···O_{NO2} short contacts.

CSD refcode	Contact	Distance, Å (Nc)	Comments
FAFWUG	Ni···O	2.930(12) (0.93)	intermolecular neutral complex
JAFKEK	Pd···O	3.094(4) (0.98)	intermolecular neutral complex
NEGNOE	Pd···O	2.941(5) (0.93)	intermolecular cationic complex
NOPYEW	Pd···O	3.114(7) (0.99)	intermolecular cationic complex
PAHVEB	Pd···O	2.944(3) (0.93)	intermolecular tetrameric cationic complex
PAHVIF	Pd···O	3.090(6) (0.98)	intermolecular tetrameric cationic complex
SEGMEW	Ni····O	3.095(15) (0.98)	intermolecular coordination polymer
UDUXUN	Ni····O	2.941(4) (0.93)	intermolecular cationic complex
UFAXOP	Pd···O	3.113(17) (0.99)	intermolecular cationic complex
WOWQUW	Pd···O	2.896(4) (0.92)	intermolecular cationic coordination polymer
VUPGEV	Ni···O	2.826(13) (0.90)	intramolecular coordination polymer
DUZVID	Pt···O	3.061(6) (0.94)	intramolecular neutral complex
EBUGOY	Pt···O	3.187(4) (0.97)	intramolecular anionic complex
EBUGUE	Pt···O	3.084(5) (0.94)	intramolecular neutral complex
EBUHAL	Pt···O	3.060(2) (0.94)	intramolecular neutral complex
EBUHEP	Pt···O	3.2191(16) (0.98)	intramolecular neutral complex
FUNLAB	Pd···O	2.888(4) (0.92)	intramolecular neutral complex
KULKIM	Pt···O	3.0457(19) (0.93)	intramolecular neutral complex
QENNUT	Pt···O	2.918(2) (0.89)	intramolecular neutral complex
QENPIJ	Pt···O	3.055(8) (0.93) 3.081(8) (0.94) 3.233(7) (0.99) 3.071(7) (0.94)	intramolecular neutral complex
QENPOP	Pt···O	3.082(2) (0.94)	intramolecular

			neutral complex
QENPUV	Pt···O	3.2429(18) (0.99)	intramolecular neutral complex
QENQIK	Pt···O	3.0357(16) (0.93)	intramolecular neutral complex
VESXOG	Ni···O	2.892(9) (0.92)	intramolecular cationic complex
SANWAJ	Pd···O	2.8462(17) (0.90)	intramolecular neutral complex
SANWEN	Pd···O	3.098(4) (0.98)	intramolecular neutral complex
AJUXAG	Ni···O	3.071(3) (0.97)	intramolecular neutral complex
AJUXEK	Ni···O	2.918(2) (0.93)	intramolecular neutral complex
AKAMOQ	Ni···O	2.515(6) (0.80)	intramolecular neutral cluster
AKUNEA	Pd···O	2.831(9)–2.907(4) (0.90)	intramolecular neutral complex
CEMKOU	Pt···O	2.9029(19) (0.89) 3.015(12) (0.92)	intramolecular neutral complex
DUPZIY	Ni···O	2.560(4) (0.81)	intramolecular neutral complex
EBUHUF	Pt···O	3.1368(18) (0.96)	intramolecular neutral complex
FIPHAN	Pd···O	2.894(8) (0.92)	intramolecular neutral complex
FULTUC	Ni···O	2.833(3) (0.90)	intramolecular neutral complex
HAKQIW	Pd···O	2.854(2) (0.91)	intramolecular neutral complex
HIPDUF	Pd···O	2.865(4) (0.91)	intramolecular cationic complex
KEPNIE	Ni···O	2.870(3) (0.91) 3.063(3) (0.97)	intramolecular neutral complex
KESLEC	Pd···O	2.829(2) (0.90)	intramolecular neutral complex
KOMKEC	Pt···O	3.12(1) (0.95)	intramolecular neutral complex
KULJAD	Pt···O	3.211(4) (0.98)	intramolecular neutral complex
KULJIL	Pt···O	3.237(9) (0.99) 3.181(10) (0.97)	intramolecular neutral complex
KUZSAZ	Pd···O	2.784(12) (0.88) 2.828(15) (0.90)	intramolecular cationic complex
LATMUO	Pt···O	3.164(18) (0.97)	intramolecular neutral complex

NAYHOK	Pd···O	3.099(7) (0.98)	intramolecular neutral complex
NAYHOK01	Pd···O	3.105(5) (0.99)	intramolecular neutral complex
QENPAB	Pt···O	3.183(2) (0.99)	intramolecular neutral complex
QENQAC	Pt···O	3.1703(16) (0.97)	intramolecular neutral complex
QENQOQ	Pt···O	3.0532(17) (0.93)	intramolecular neutral complex
SALNEY	Pd···O	2.910(3) (0.92) 2.911(3) (0.92)	intramolecular anionic complex
VINBUP	Pd···O	2.85(3) (0.90) 2.81(2) (0.89)	intramolecular neutral complex
VOKPOA	Pd···O	2.756(6) (0.87)	intramolecular cationic complex
WOSYIM	Pd···O	2.991(9) (0.95)	intramolecular neutral complex
YASNUB	Pt···O	3.112(7) (0.95) 3.090(8) (0.94)	intramolecular neutral complex
YOBNOT	Pd···O	3.0061(16) (0.95)	intramolecular neutral complex
YOBNUZ	Pd···O	3.017(2) (0.96)	intramolecular neutral complex
YOBPEL	Pd···O	3.006(4) (0.95) 2.972(4) (0.94) 3.033(3) (0.95) 3.004(3) (0.95) 3.078(4) (0.98) 3.103(4) (0.99)	intramolecular neutral complex
YOBPIP	Pt···O	2.994(3) (0.92) 3.146(3) (0.96)	intramolecular neutral complex
ZAXXII	Ni···O	3.069(3) (0.97)	intramolecular neutral complex
ZIVZUB	Pd···O	2.954(3) (0.94)	intramolecular neutral complex
AWOMIJ	Pt···O	3.271(8) (1.01)	intermolecular* cationic complex
MALHEN	Pt···O	3.401(3) (1.05)	intermolecular* cationic complex
TOKHIM	Pt···O	3.351(2) (1.03)	intermolecular* cationic complex

Hereinafter Nc is normalized contact distance, Nc = d/Σ_{BvdW} or d/Σ_{AvdW}, where Σ_{BvdW} is Bondi van der Waals radii[5] sum for interacting atoms: Σ_{BvdW}(Ni,O) = 3.15; Σ_{BvdW}(Pd,O) = 3.15 Å; Σ_{BvdW}(Pt,O) = 3.27 Å.

*Criterium distance (Pt–O) ≤ (Σ_{vdW} + 0.21 Å) (3.45 Å) was used for selection.

Table S5. CSD data for complexes bearing metal-bound NO_2-group.

CSD refcode	Bond	Bond length, Å	Comments
AMOBEM	Ni–O	2.142(6)	NO_2 in 6-membered chelate ring, Ni^{II}, O
CEFHAW	Pt–O	2.0604(8)	NO_2 in 5-membered chelate ring, Pt^{II}, SP
DOBZOJ	Ni–O	2.087(5)	NO_2 in 6-membered chelate ring, Ni^{II}, O
DUZVID	Pt–O	2.138(5)	NO_2 in 5-membered chelate ring, Pt^{II}, SP + short contact Pt···O
EBUGOY	Pt–O	2.088(3)	NO_2 in 5-membered chelate ring, Pt^{II}, SP + short contact Pt···O
EBUGUE	Pt–O	2.067(4)	NO_2 in 5-membered chelate ring, Pt^{II}, SP + short contact Pt···O
EBUHAL	Pt–O	2.0739(19)	NO_2 in 5-membered chelate ring, Pt^{II}, SP + short contact Pt···O
EBUHEP	Pt–O	2.0843(16)	NO_2 in 5-membered chelate ring, Pt^{II}, SP + short contact Pt···O
EBUHIT	Pt–O	2.254(5) 2.068(3)	NO_2 in 5-membered chelate ring, Pt^{II}, O with Pt–Hg bond
EBUHOZ	Pt–O	2.283(3) 2.071(3)	NO_2 in 5-membered chelate ring, Pt^{II}, O with Pt–Hg bond
FEVBAJ	Ni–O	2.0509(17)	NO_2 in 6-membered chelate ring, Ni^{II}, O
FEVPUR	Pt–O	2.166(4) 2.173(4)	NO_2 in 5-membered chelate ring, Pt^{IV}, O
FUNKUU	Pd–O	2.130(5) 2.158(6)	NO_2 in 5-membered chelate ring, Pd^{II}, SP
FUNLAB	Pd–O	2.137(3)	NO_2 in 5-membered chelate ring, Pd^{II}, SP + short contact Pd···O
GUNLAF	Ni–O	2.174(3)	NO_2 in 6-membered chelate ring, Ni^{II}, O
HIPDIT	Pd–O	2.014(2)	NO_2 in 5-membered chelate ring, Pd^{II}, SP
KULHEF	Pt–O	1.999(4)	NO_2 in 5-membered chelate ring, Pt^{II}, SP
KULHIJ	Pt–O	1.990(5)	NO_2 in 5-membered chelate ring, Pt^{II}, SP
KULKAE	Pt–O	2.035(4) 2.098(4)	NO_2 in 5-membered chelate ring, Pt^{IV}, O
KULKEI	Pt–O	2.021(5)	NO_2 in 5-membered chelate

		2.035(5)	ring, Pt^{IV}, O
KULKIM	Pt–O	2.0781(15)	NO_2 in 5-membered chelate ring, Pt^{II}, SP + Pt···O contact
KULKOS	Pt–O	2.080(3)	NO_2 in 5-membered chelate ring, Pt^{II}, SP
MECRAN	Ni–O	2.117(4)	NO_2 in 6-membered chelate ring, Ni^{II}, O
QENNUT	Pt–O	2.0769(17)	NO_2 in 5-membered chelate ring, Pt^{II}, SP
QENPIJ	Pt–O	2.049(6) 2.045(6) 2.055(6) 2.039(6)	NO_2 in 5-membered chelate ring, Pt^{II}, SP + Pt···O contact
QENPOP	Pt–O	2.079(2)	NO_2 in 5-membered chelate ring, Pt^{II}, SP + Pt···O contact
QENPUV	Pt–O	2.0747(16)	NO_2 in 5-membered chelate ring, Pt^{II}, SP + Pt···O contact
QENQIK	Pt–O	2.0789(18)	NO_2 in 5-membered chelate ring, Pt^{II}, SP + Pt···O contact
RAQKUR	Ni–O	2.042(3) 2.067(3)	monodentate $MeNO_2$, Ni^0 (in $[Ni(MeNO_2)_2(Et_2O)(lin\text{-}NO)](PF_6)$), distorted T
TAQFUO	Ni–O	2.033(6) 2.050(4) 2.054(3)	monodentate $MeNO_2$, Ni^0 (in $[Ni(MeNO_2)_3(lin\text{-}NO)](PF_6)$), distorted T
TETZAW	Ni–O	2.136(4) 2.171(3)	NO_2 in 6-membered chelate ring, Ni^{II}, O
TETZEA	Ni–O	2.123(7) 2.100(7)	NO_2 in 6-membered chelate ring, Ni^{II}, O
YOBPUB	Pd–O	2.019(3)	NO_2 in 5-membered chelate ring, Pd^{II}_2, TP with Pd-Pd bond
ZETWEE	Ni–O	2.052(5) 2.056(4) 2.033(5) 2.057(4) 2.045(3) 2.057(4)	NO_2 in 6-membered chelate ring, Ni^{II}, O
ZOMYEI	Pd–O	2.2782(14)	monodentate RNO_2, Pt^{II}, SP

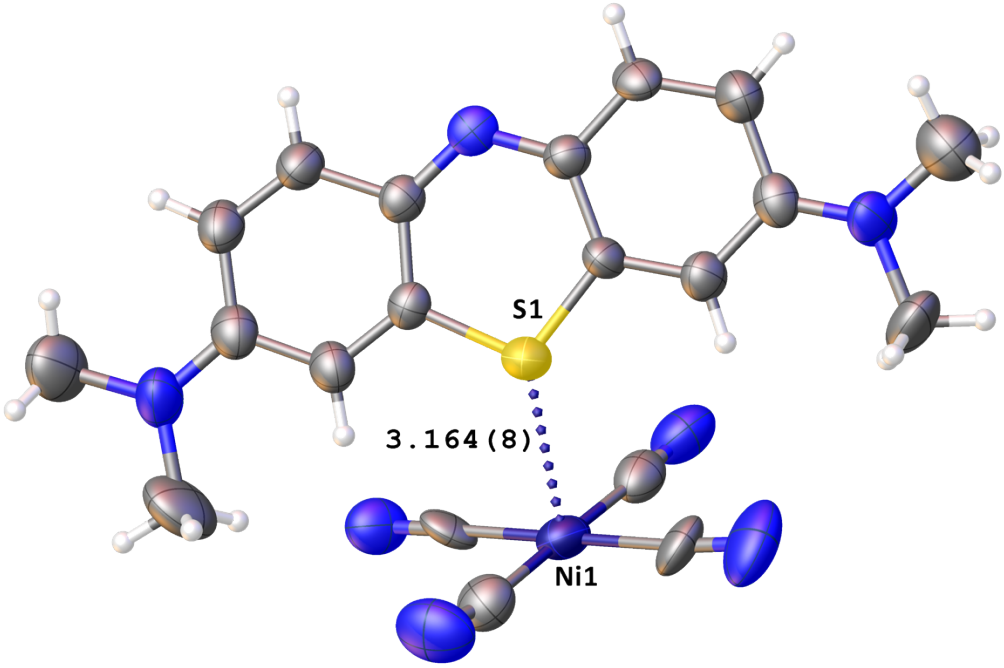

Figure S18. View of the structure KUMWIB, demonstration intermolecular contact Ni···S.

S5. Theoretical studies

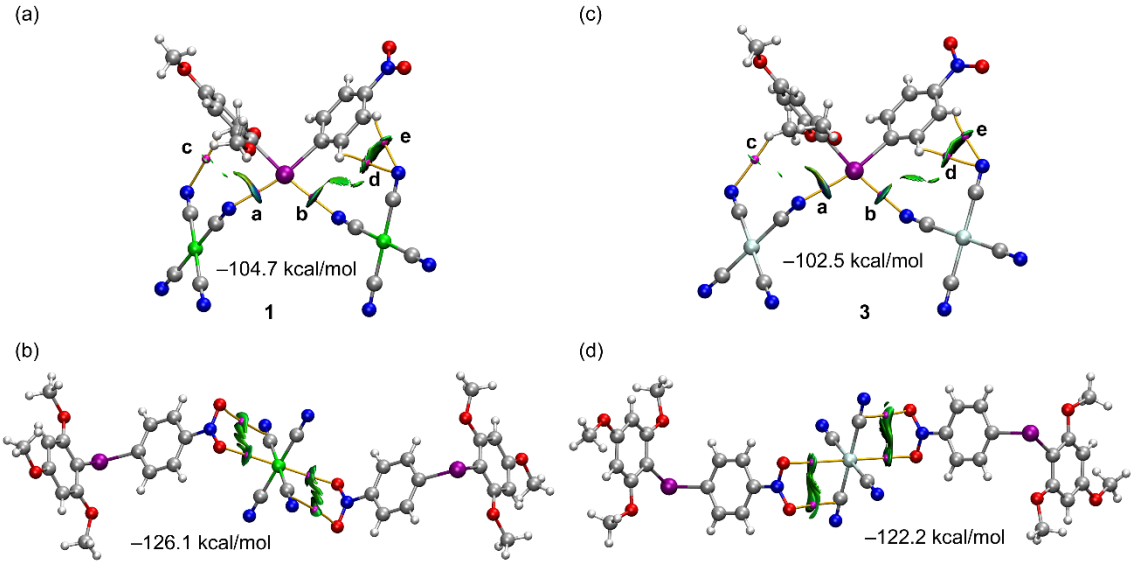

Figure S19. QTAIM (bond CPs in red and bond paths as solid lines) and NCIplot (see theoretical methods for settings) of the halogen bonded (a,c) and Pd···O_{NO2} (b,d) bonded trimers of compounds **1** (left) and **3** (right). Only intermolecular contacts are shown. The interaction energies are also indicated.

S6. Crystallization and characterization of 1–3

Crystallization of [{2,4,6-(MeO)$_3$C$_6$H$_2$}(4-NO$_2$-C$_6$H$_4$)I]$_2$[M(CN)$_4$] (1–3). A solution of any one of (PPN)$_2$[M(CN)$_4$] (15.5 μmol) in MeNO$_2$ (for **2** and **3**) or CH$_2$Cl$_2$ (for **1**) (2 mL) was added to a solution of [{2,4,6-(MeO)$_3$C$_6$H$_2$}(4-NO$_2$-C$_6$H$_4$)I](CF$_3$CO$_2$) (31.0 μmol) in MeNO$_2$ or CH$_2$Cl$_2$ (2 mL) and the resulting homogeneous solution was left to stand for several days at room temperature for slow evaporation, whereupon a few crystals suitable for XRD were manually separated. Solid residues were dried in air at RT. The presence of halogens (iodine in our particular case) in any structure spoils the column of an analyzer and, and usually leads to poorly reproducible data. In addition to the XRD, we characterized the obtained compounds using FTIR (in KBr) and ATR-FTIR spectroscopy and HRESI mass-spectrometry. All species exhibit peaks from the iodonium cation [2,4,6-(MeO)$_3$C$_6$H$_2$/4-NO$_2$-C$_6$H$_4$I]$^+$ in their positive mode mass-spectra and also peaks of the dianion [M(CN)$_4$]$^{2-}$ and its fragmentation ion, [M(CN)$_3$]$^-$, in the negative mode mass-spectra.

1. IR (KBr, selected bands, cm^{-1}): 3094, 3011 w ν(C$_{Ar}$–H), 2949, 2851 w ν(C$_{Me}$–H), 2115 and 2105 s ν(C≡N), 1586 s ν(CC$_{Ar}$), 1529 s ν(NO$_2$ asym), 1468 m-s ν(CC$_{Ar}$), 1343 s ν(NO$_2$ sym), 1229 s, 1207 m-s and 1124 s ν(C–O), 849 m-s ν(C–N) and/or δ(C$_{Ar}$–H), 736 m-s δ(C$_{Ar}$–H). ATR-FTIR (selected bands, cm^{-1}): 3099, 3011 w ν(C$_{Ar}$–H), 2950, 28521 w ν(C$_{Me}$–H), 2114 and 2105 s ν(C≡N), 1582 s ν(CC$_{Ar}$), 1526 s ν(NO$_2$ asym), 1468 m-s ν(CC$_{Ar}$), 1343 s ν(NO$_2$ sym), 1227 s, 1206 m-s and 1123 s ν(C–O), 849 m-s ν(C–N) and/or δ(C$_{Ar}$–H), 736 m-s δ(C$_{Ar}$–H). HRESI$^+$-MS: *m/z*: 415.9983 [{2,4,6-(MeO)$_3$C$_6$H$_2$}(4-NO$_2$-C$_6$H$_4$)I]$^+$ (calcd 415.9989). HRESI$^-$-MS: *m/z*: 135.9456 [Ni(CN)$_3$]$^-$ (calcd 135.9451).

2. IR (KBr, selected bands, cm^{-1}): 3092, 3011 w ν(C$_{Ar}$–H), 2949, 2852 w ν(C$_{Me}$–H), 2129 and 2120 s ν(C≡N), 1586 s ν(CC$_{Ar}$), 1529 m-s ν(NO$_2$ asym), 1469 m-s ν(CC$_{Ar}$), 1343 s ν(NO$_2$ sym), 1229 s, 1207 m-s and 1124 s ν(C–O), 850 m-s ν(C–N) and/or δ(C$_{Ar}$–H), 736 m δ(C$_{Ar}$–H). ATR (selected bands, cm^{-1}): 3094, 3012 w ν(C$_{Ar}$–H), 2949, 2851 w ν(C$_{Me}$–H), 2129 and 2119 s ν(C≡N), 1584 s ν(CC$_{Ar}$), 1528 m-s ν(NO$_2$ asym), 1470 m-s ν(CC$_{Ar}$), 1344 s ν(NO$_2$ sym), 1229 s, 1207 m-s

and 1123 s ν(C–O), 849 m-s ν(C–N) and/or δ(C_{Ar}–H), 737 m δ(C_{Ar}–H). HRESI$^+$-MS: *m/z*: 415.9985 [{2,4,6-$(MeO)_3C_6H_2$}(4-NO_2-C_6H_4)I]$^+$ (calcd 415.9989). HRESI$^-$-MS: *m/z*: 104.9579 $[Pd(CN)_4]^{2-}$ (calcd 104.9585), 183.9136 $[Pd(CN)_3]^-$ (calcd 183.9134).

3. IR (KBr, selected bands, cm^{-1}): 3092, 3011 w ν(C_{Ar}–H), 2949, 2924, 2851 w ν(C_{Me}–H), 2116(sh) s ν(C≡N), 1586 s ν(CC_{Ar}), 1530 m-s ν(NO_2 asym), 1470 m-s ν(CC_{Ar}), 1344 s ν(NO_2 sym), 1229 s, 1207 m-s and 1124 s ν(C–O), 849 m-s ν(C–N) and/or δ(C_{Ar}–H), 736 m δ(C_{Ar}–H). ATR (selected bands, cm^{-1}): 3092, 3012 w ν(C_{Ar}–H), 2949, 2924, 2851 w ν(C_{Me}–H), 2124 and 2116 s ν(C≡N), 1585 s ν(CC_{Ar}), 1529 m-s ν(NO_2 asym), 1469 m-s ν(CC_{Ar}), 1343 s ν(NO_2 sym), 1229 s, 1207 m-s and 1123 s ν(C–O), 849 m-s ν(C–N) and/or δ(C_{Ar}–H), 736 m δ(C_{Ar}–H). HRESI$^+$-MS: *m/z*: 415.9887 [{2,4,6-$(MeO)_3C_6H_2$}(4-NO_2-C_6H_4)I]$^+$ (calcd 415.9989). HRESI$^-$-MS: *m/z*: 149.4895 $[Pt(CN)_4]^{2-}$ (calcd 149.4891), 272.9742 $[Pt(CN)_3]^-$ (calcd 272.9740).

S7. Experimental data

Figure S20. IR spectrum of **1** in KBr.

Figure S21. ATR-FTIR spectrum of **1**.

Figure S22. IR spectrum of **2** in KBr.

Figure S23. ATR-FTIR spectrum of **2**.

Figure S24. IR spectrum of **3** in KBr.

Figure S25. ATR-FTIR spectrum of **3**.

$[Ar^1Ar^2I](CF_3CO_2)$, IR in NaCl (*lit.*[6]): 3098 w, 2449 w, 1664 s, 1520 s, 1347 s.

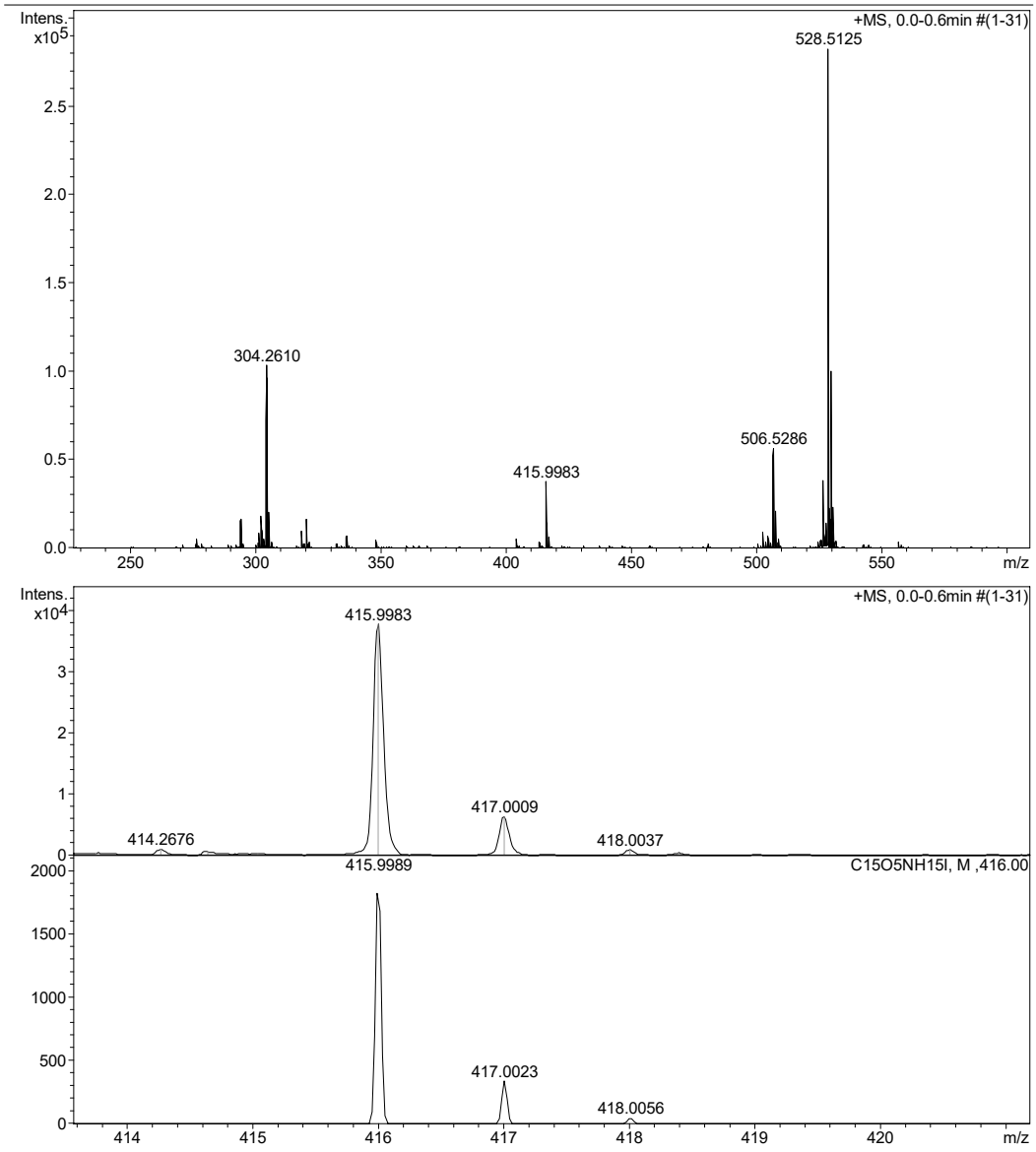

Figure S26. High resolution ESI-MS$^+$ spectrum of **1**.

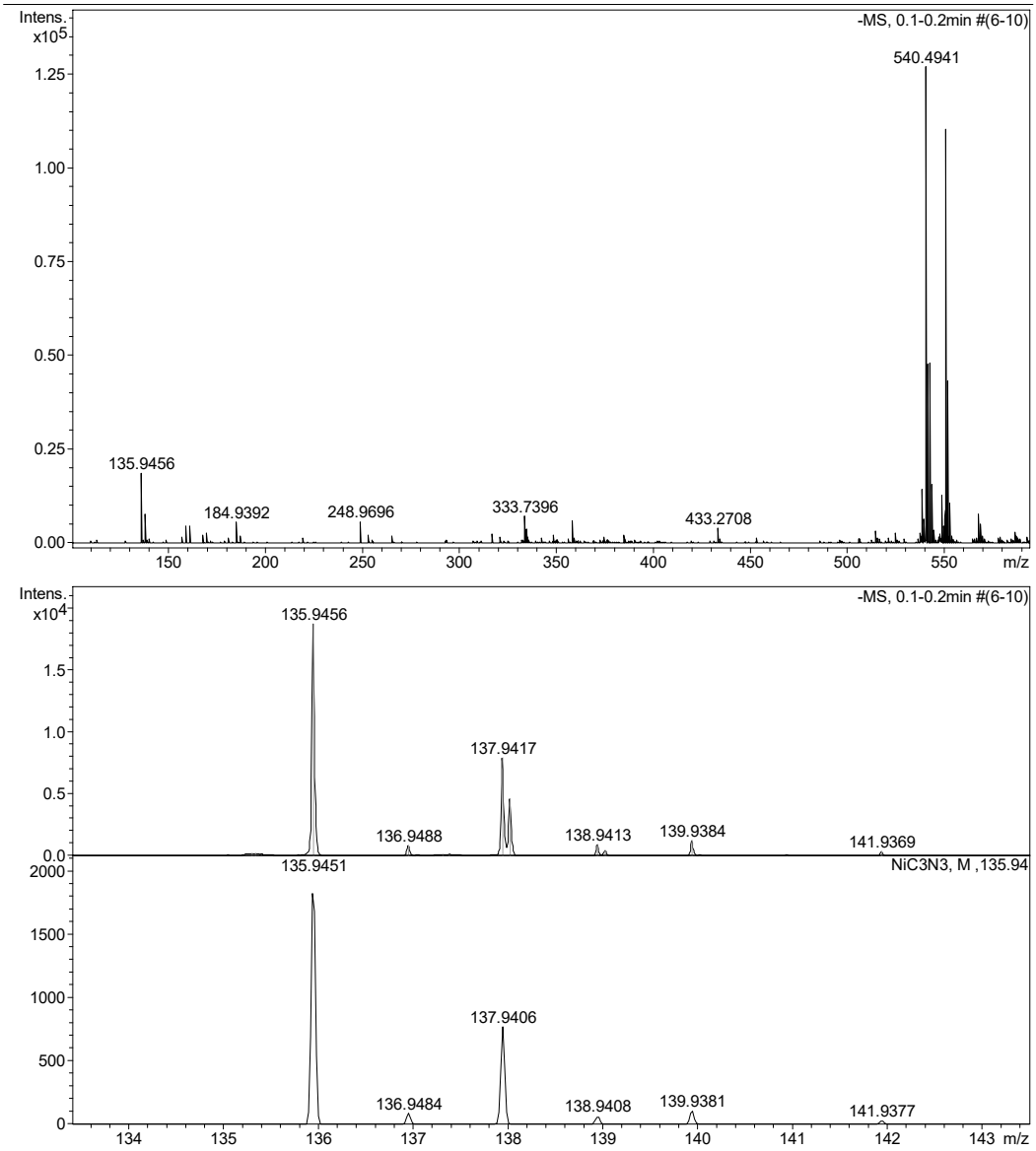

Figure S27. High resolution ESI-MS$^-$ spectrum of **1**.

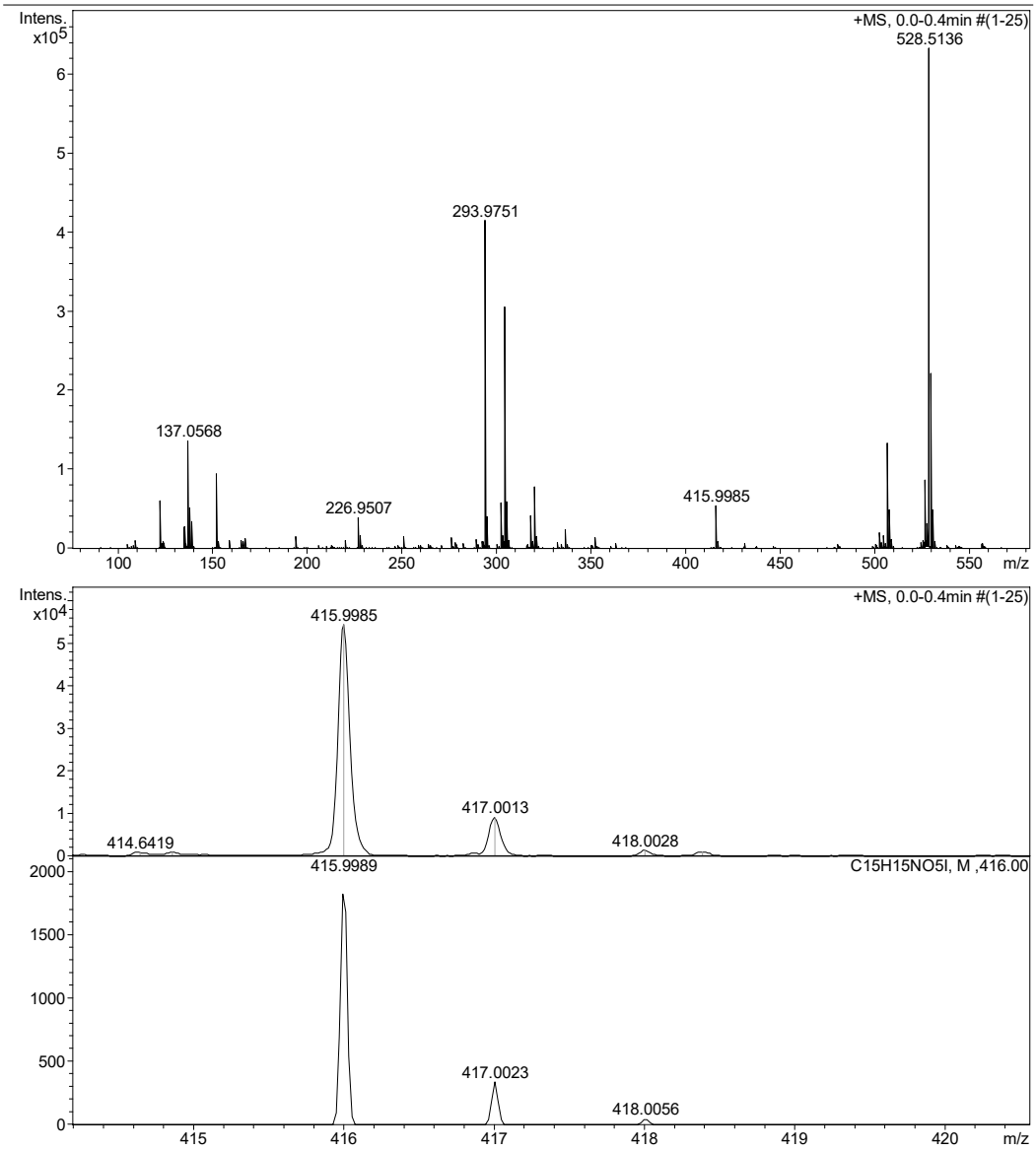

Figure S28. High resolution ESI-MS$^+$ spectrum of **2**.

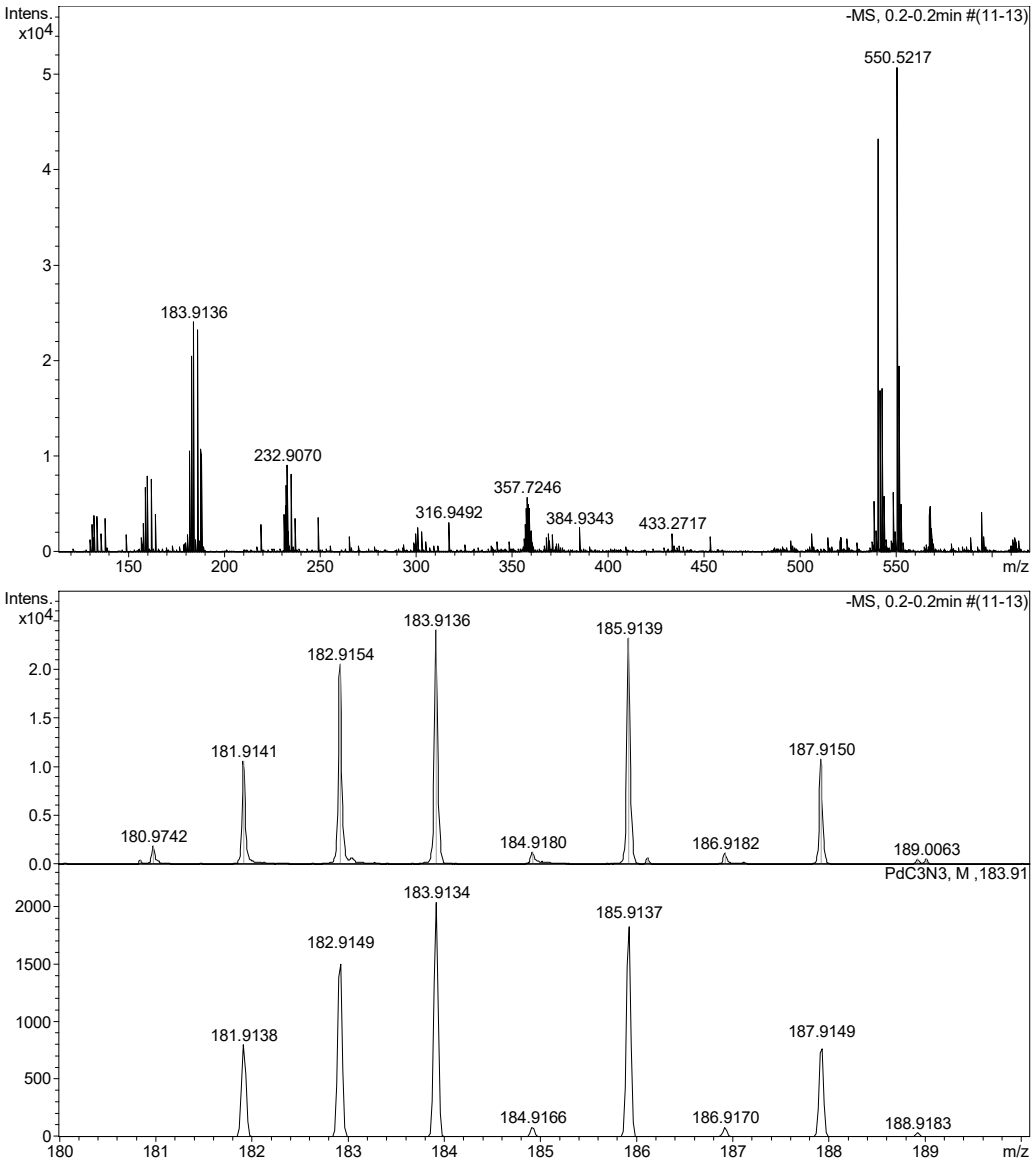
Intens.
x10^4
-MS, 0.2-0.2min #(11-13)
550.5217
183.9136
232.9070
357.7246
316.9492
384.9343
433.2717
m/z
Intens.
x10^4
-MS, 0.2-0.2min #(11-13)
183.9136
185.9139
182.9154
181.9141
187.9150
180.9742
184.9180
186.9182
189.0063
PdC3N3, M ,183.91
183.9134
185.9137
182.9149
181.9138
187.9149
184.9166
186.9170
188.9183
m/z

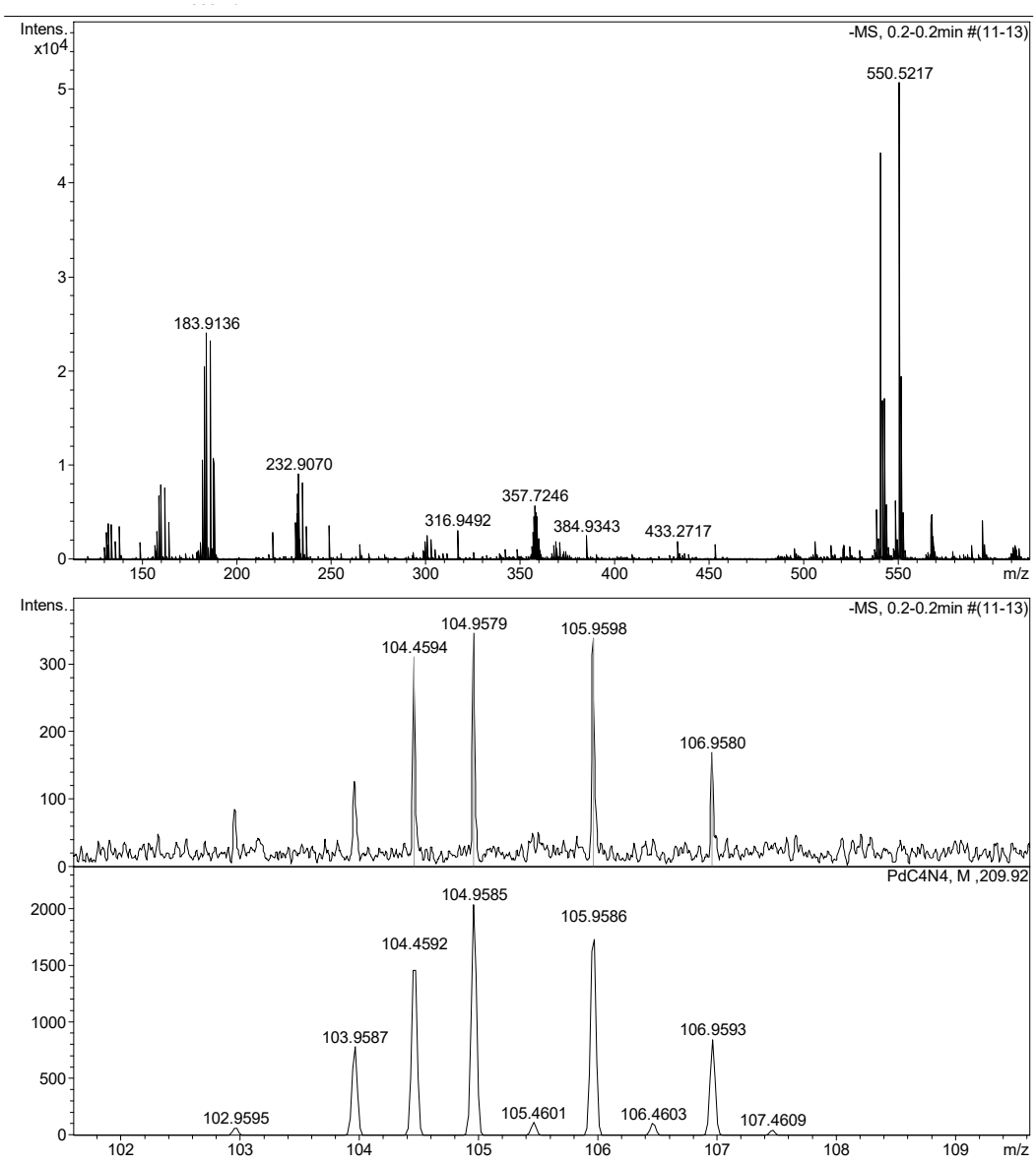

Figure S29. High resolution ESI-MS$^-$ spectrum of **2**.

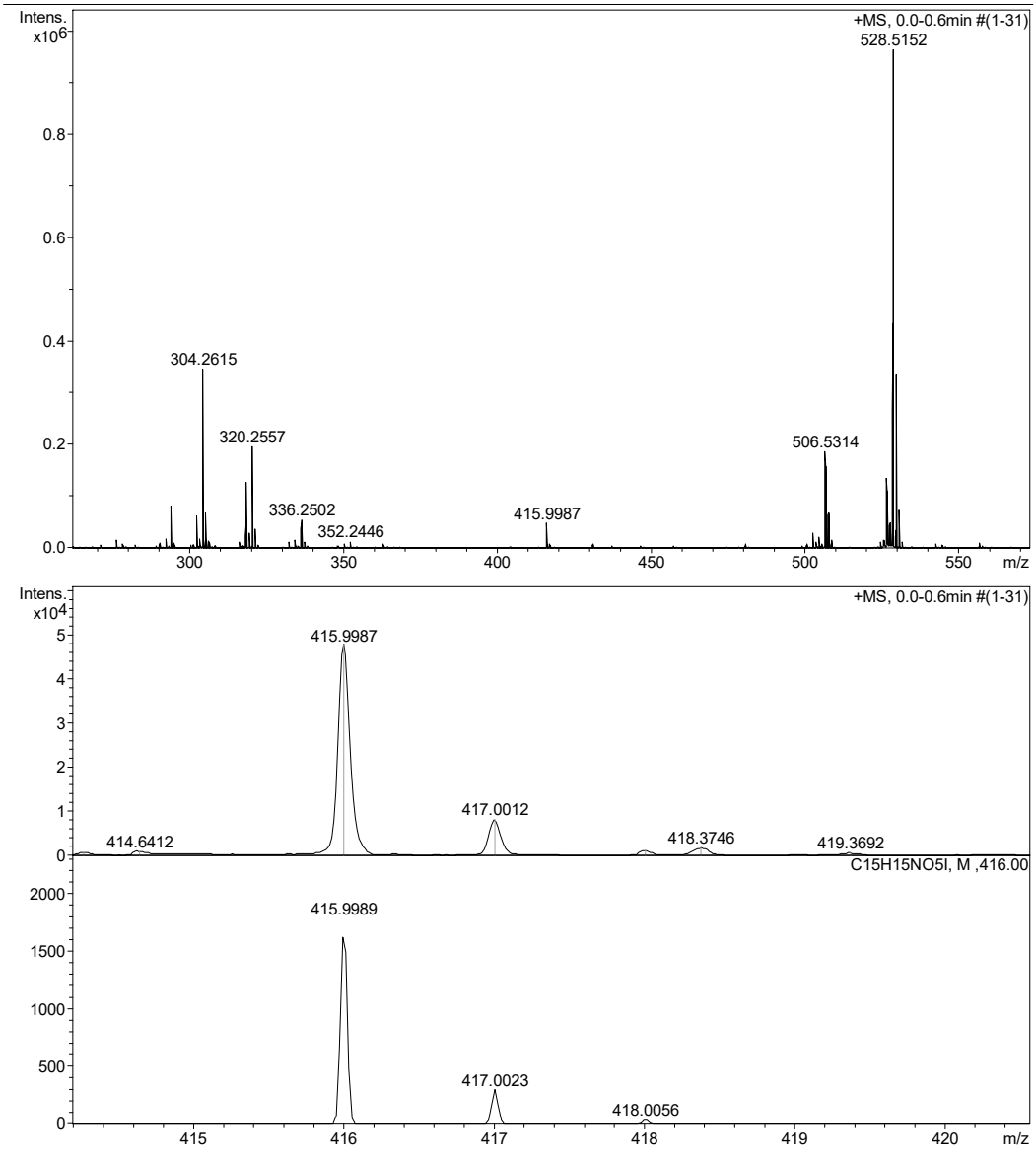

Figure S30. High resolution ESI-MS$^+$ spectrum of **3**.

Display Report

Analysis Info

Analysis Name	D:\Data\2023\February\20\SVV_155-.d	Acquisition Date	20.02.2023 16:13:29
Method	tune_low.m	Operator	Bruker Customer
Sample Name		Instrument / Ser#	micrOTOF 10223
Comment			

Acquisition Parameter

Source Type	ESI	Ion Polarity	Negative	Set Nebulizer	0.6 Bar
Focus	Not active			Set Dry Heater	180 °C
Scan Begin	21 m/z	Set Capillary	4500 V	Set Dry Gas	6.0 l/min
Scan End	1000 m/z	Set End Plate Offset	-500 V	Set Divert Valve	Source

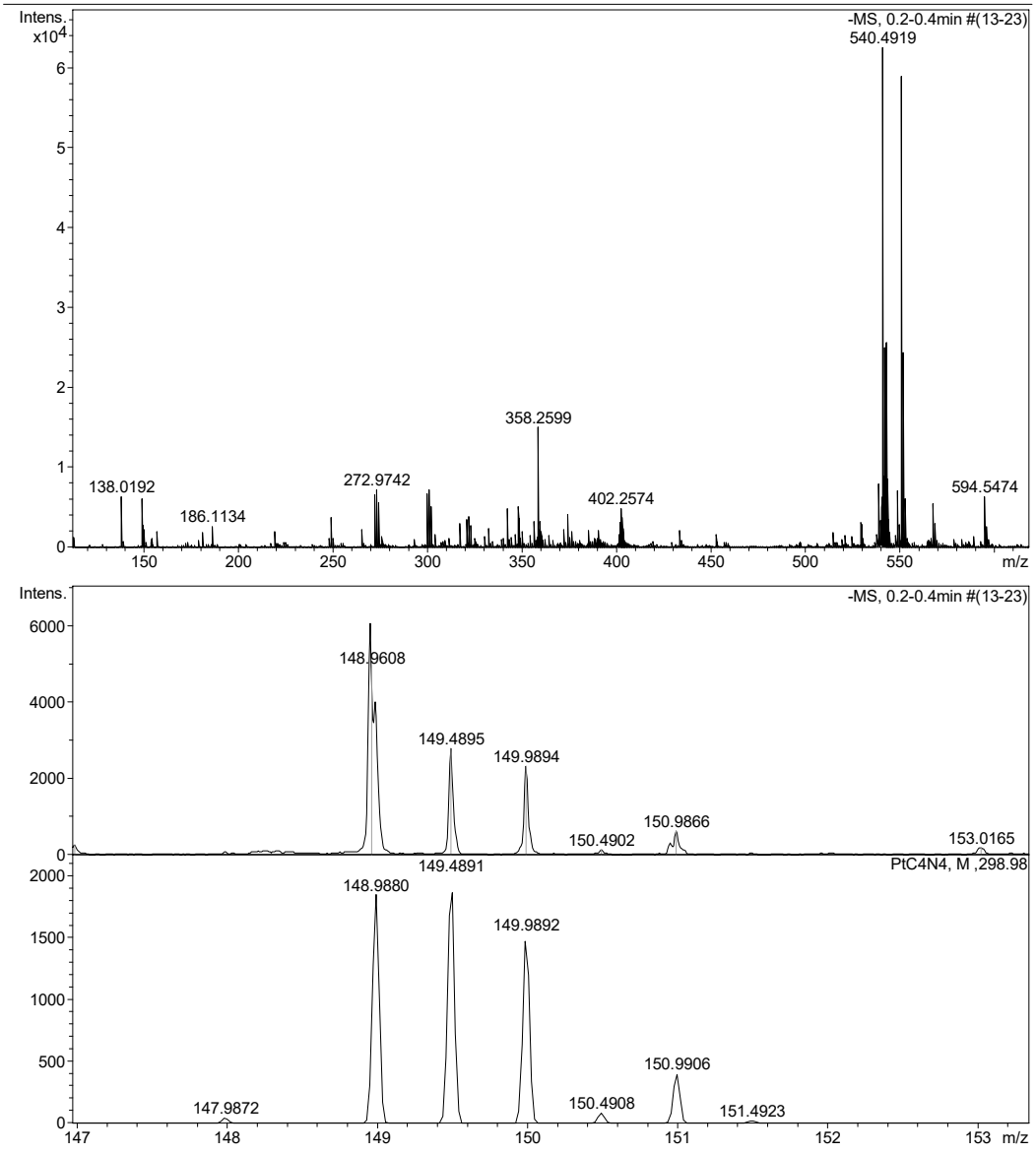

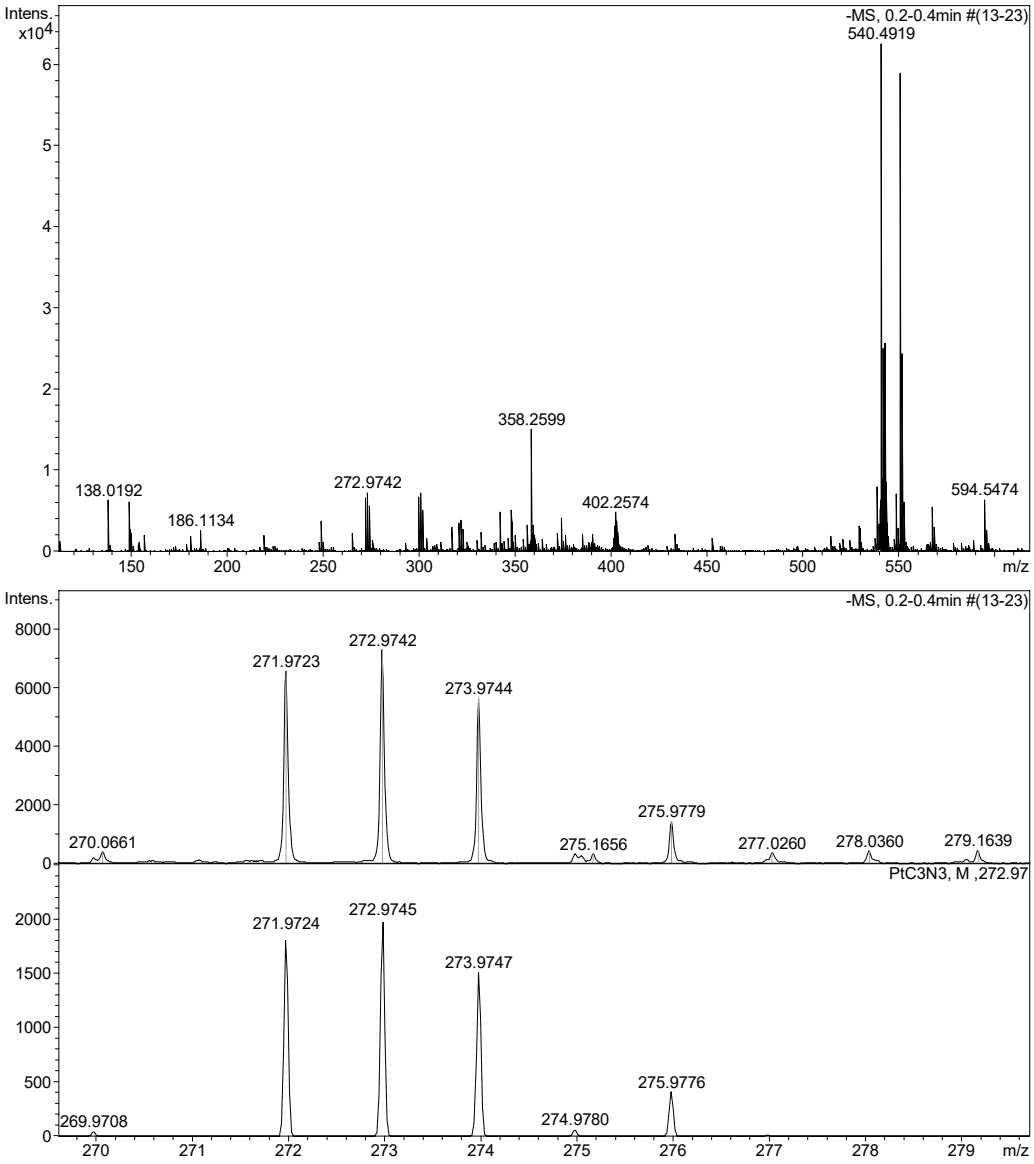

Figure S31. High resolution ESI-MS$^-$ spectrum of **3**.

References

1. V. V. Suslonov, N. S. Soldatova, P. S. Postnikov, G. Resnati, V. Y. Kukushkin, D. M. Ivanov and N. A. Bokach, Diaryliodonium Tetracyanidometallates Self-Assemble into Halogen-Bonded Square-Like Arrays, *Crystal Growth & Design*, 2022, **22**, 2749-2758.
2. V. V. Suslonov, A. A. Eliseeva, A. S. Novikov, D. M. Ivanov, A. Y. Dubovtsev, N. A. Bokach and V. Y. Kukushkin, Tetrachloroplatinate(II) anion as a square-planar tecton for crystal engineering involving halogen bonding, *Crystengcomm*, 2020, **22**, 4180-4189.
3. V. V. Suslonov, N. S. Soldatova, D. M. Ivanov, B. Galmés, A. Frontera, G. Resnati, P. S. Postnikov, V. Y. Kukushkin and N. A. Bokach, Diaryliodonium Tetrachloroplatinates(II): Recognition of a Trifurcated Metal-Involving μ3-I···(Cl,Cl,Pt) Halogen Bond, *Crystal Growth & Design*, 2021, **21**, 5360-5372.
4. G. R. Desiraju, P. S. Ho, L. Kloo, A. C. Legon, R. Marquardt, P. Metrangolo, P. Politzer, G. Resnati and K. Rissanen, Definition of the halogen bond (IUPAC Recommendations 2013), *Pure Appl. Chem.*, 2013, **85**, 1711.
5. A. Bondi, Van der Waals Volumes and Radii, *J. Phys. Chem.*, 1964, **68**, 441–451.
6. A. H. Sandtorv and D. R. Stuart, Metal-free Synthesis of Aryl Amines: Beyond Nucleophilic Aromatic Substitution, *Angewandte Chemie International Edition*, 2016, **55**, 15812-15815.